Topological Surface States with Persistent High Spin Polarization across the Dirac Point in Bi_2Te_2Se and Bi_2Se_2Te

K. Miyamoto,[1,*] A. Kimura,[2] T. Okuda,[1] H. Miyahara,[2] K. Kuroda,[2] H. Namatame,[1] M. Taniguchi,[1,2] S. V. Eremeev,[3,4] T. V. Menshchikova,[4] E. V. Chulkov,[5,6] K. A. Kokh,[7] and O. E. Tereshchenko[8,9]

[1]*Hiroshima Synchrotron Radiation Center, Hiroshima University, 2-313 Kagamiyama, Higashi-Hiroshima 739-0046, Japan*
[2]*Graduate School of Science, Hiroshima University, 1-3-1 Kagamiyama, Higashi-Hiroshima 739-8526, Japan*
[3]*Institute of Strength Physics and Materials Science, 634021, Tomsk, Russia*
[4]*Tomsk State University, 634050, Tomsk, Russia*
[5]*Donostia International Physics Center (DIPC), 20018 San Sebastián/Donostia, Basque Country, Spain*
[6]*Departamento de Física de Materiales UPV/EHU, Centro de Física de Materiales CFM—MPC and Centro Mixto CSIC-UPV/EHU, 20080 San Sebastián/Donostia, Basque Country, Spain*
[7]*V.S. Sobolev Institute of Geology and Mineralogy, Siberian Branch, Russian Academy of Sciences, Koptyuga pr. 3, Novosibirsk, 630090 Russia*
[8]*Institute of Semiconductor Physics, Siberian Branch, Russian Academy of Sciences, pr. Akademika Lavrent'eva 13, Novosibirsk, 630090 Russia*
[9]*Novosibirsk State University, ul. Pirogova 2, Novosibirsk, 630090 Russia*

(Received 20 March 2012; published 17 October 2012)

Helical spin textures with marked spin polarizations of topological surface states have been unveiled for the first time by state-of-the-art spin- and angle-resolved photoemission spectroscopy for two promising topological insulators, Bi_2Te_2Se and Bi_2Se_2Te. Their highly spin-polarized natures are found to be persistent across the Dirac point in both compounds. This novel finding paves a pathway to extending the utilization of topological surface states of these compounds for future spintronic applications.

DOI: 10.1103/PhysRevLett.109.166802 PACS numbers: 73.20.−r, 71.70.Ej, 79.60.−i

Three-dimensional topological insulators (3D TIs) with massless helical Dirac fermions at the surface in a bulk energy gap induced by strong spin-orbit coupling have attracted a great deal of attention as key materials to revolutionize current electronic devices [1–4]. A spin helical texture of a topological surface state (TSS), where the electron spin is locked to its momentum, is a manifestation of a 3D TI, which is clearly distinguished from the real-spin degenerate Dirac cone in graphene. This situation promises an effective spin polarized current in an electric field as well as a substantial suppression of backscattering in the presence of nonmagnetic impurities. These new states of matter are also expected to provide fertile ground to realize new phenomena in condensed matter physics, such as a magnetic monopole arising from the topological magnetoelectric effect and Majorana fermions hosted by hybrids with superconductors [5,6].

A number of 3D TIs, such as Bi_2Te_3 [7], Bi_2Se_3 [8–10], and thallium-based compounds [11–16], were predicted and experimentally realized. Among the established 3D TIs, the binary tetradymite compounds, Bi_2Se_3 and Bi_2Te_3 have been most extensively studied because of their relatively large energy gap and the simplest TSS. The spin-momentum locking feature has been experimentally proved at least for the upper-lying TSS by spin- and angle-resolved photoemission spectroscopy (SARPES) with widely spread values of raw spin polarizations (20–80%) [9,17–21], but clear spin polarizations are obscured near and below the Dirac point (E_D). Scanning tunneling spectroscopy for Bi_2Se_3 under a perpendicular magnetic field has revealed the presence of Landau levels (LLs) with the energy separation being proportional to $\sqrt{|n|B}$, where n and B denote the LL index and the magnetic field. The observation of these LLs evidently signifies the existence of a surface Dirac cone. However, such characteristic LLs are missing below E_D [22,23]. These features obviously tell us that the topological nature of the material survives only in the upper part of the TSS but is no longer available below E_D in Bi_2Se_3 and Bi_2Te_3. The absence of such a topological nature at TSS below E_D could be a disadvantage for extending its spintronic applications. Furthermore, in spite of significant efforts to realize surface isolated transport, progress has thus been hampered by a tiny surface contribution to the total conductance [24–27] because uncontrolled bulk carrier doping takes place in Bi_2Se_3 and Bi_2Te_3 due to the Se vacancy and the Bi-Te antisite defect.

Recently, one of the ternary tetradymite compounds, Bi_2Te_2Se, where the central Te layer is replaced by an Se layer in Bi_2Te_3, was shown to be a 3D TI by the angle-resolved photoemission spectroscopy (ARPES) measurement [28,29]. Importantly, suppression of the bulk conductivity is anticipated because the well-confined Se atoms in the central layer are expected to suppress the Se vacancy as well as the antisite defects between Bi and Te atoms. Actually, a highly bulk resistive feature in this compound has successfully led to the observation of its surface-derived

quantum oscillations in a magnetotransport experiment [30]. Another ternary compound Bi_2Se_2Te has also been predicted to be a 3D TI [31] and its TSS has been demonstrated by an ARPES measurement [29].

Here a question arises for these compounds: How are these spin polarized natures maintained in their TSSs? Realization of the TSS with high spin polarization over a wide energy range across E_D is crucial for ambipolar gate control of TI devices [32,33]. One can also manipulate the spin orientations by tuning the electron filling level in the TSS [Fig. 1(a)] as expected for the dual gate TI device [34]. In this Letter, we have unambiguously clarified for the first time by state-of-the-art SARPES that the ternary tetradymite compounds Bi_2Te_2Se and Bi_2Se_2Te possess spin polarized TSSs with marked spin polarizations. Importantly, their spin polarized natures in the TSS are found to be persistent even below E_D.

The crystals of Bi_2Te_2Se and Bi_2Se_2Te were grown from a presynthesized mixture of Bi_2Te_3 and Bi_2Se_3 by a modified vertical Bridgman method [35]. The purity of the elemental Bi, Te, and Se used for the synthesis of the binary compounds was 99.999%. The chemical analysis was done by energy dispersive x-ray spectroscopy. ARPES and SARPES experiments were performed with a He discharge lamp and synchrotron radiation (SR) at the Efficient SPin REsolved SpectroScOpy (ESPRESSO) end station attached to the APPLE-II type variable polarization undulator beam line (BL-9B) at the Hiroshima Synchrotron Radiation Center (HSRC) [36]. The VLEED-type spin polarimeter utilized in the ESPRESSO achieves a 100 times higher efficiency compared to that of conventional Mott-type spin detectors [36]. Photoelectron spin polarizations are measured by switching the direction of the in-plane target magnetizations, thereby simultaneously eliminating the instrumental asymmetry, which is a great advantage for the quantitative spin analysis of nonmagnetic systems as in the present case. This machine can resolve both out-of-plane (Z) and in-plane (X) spin polarization components with high angular and energy resolutions as schematically shown in Fig. 1(b). The sign of the polar (tilt) angle is defined as positive, in the case of clockwise (anticlockwise) rotation about y axis (x axis) as shown in Fig. 1(b). The overall experimental energy and wave number resolutions of ARPES (SARPES) were set to 25 meV and <0.008 Å^{-1} (25 meV and <0.04 Å^{-1}), respectively. All measurements were performed at a sample temperature of 70 K. The samples were *in situ* cleaved under ultrahigh vacuum below 1×10^{-8} Pa. DFT calculations were performed using the VASP code [37], where the interaction between the ion cores and valence electrons was described by the projector augmented wave method [38]. The generalized gradient approximation was used to describe the exchange correlation energy. The Hamiltonian contained scalar-relativistic corrections, and spin-orbit coupling was taken into account by the second variation method.

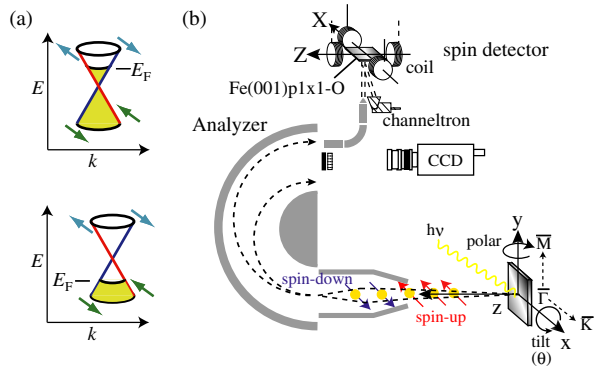

FIG. 1 (color online). (a) Schematic of the topological surface state with different filling levels. (b) Schematic of our efficient spin resolved spectroscopy (ESPRESSO) machine at HSRC and the experimental geometry.

Figures 2(a) and 2(c) show the ARPES energy dispersion curves of the TSS along the $\bar{K}$-$\bar{\Gamma}_{2nd}$-$\bar{K}$ direction for Bi_2Te_2Se and Bi_2Se_2Te taken with a He discharge lamp ($h\nu = 21.22$ eV). It is found that the TSSs for both compounds are more pronounced at $\bar{\Gamma}_{2nd}$ rather than at $\bar{\Gamma}_{1st}$ (not shown). Here, $\bar{\Gamma}_{2nd}$ ($\bar{\Gamma}_{1st}$) denotes the $\bar{\Gamma}$ point in the second

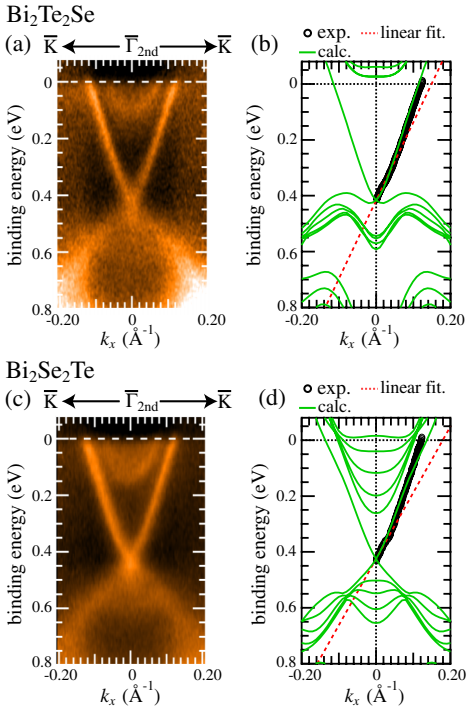

FIG. 2 (color online). (a),(c) ARPES energy dispersion curves of Bi_2Te_2Se and Bi_2Se_2Te along the $\bar{K}$-$\bar{\Gamma}_{2nd}$-$\bar{K}$ line. (b), (d) Intensity maxima plot for one TSS branch above the Dirac point obtained from momentum distribution curves (open circles) in (a) and (c), respectively. Fitted linear functions are denoted with dashed lines. Energy dispersions of Bi_2Te_2Se and Bi_2Se_2Te are compared with the results of first principles calculation in panels (b) and (d).

(first) surface Brillouin zone (SBZ). One can see that the measured dispersions of the TSS for both compounds are linear below and above E_D and become more steep approaching the conduction band. The observed TSS band dispersion for Bi_2Te_2Se in the 2nd SBZ is in agreement with those obtained from the other ARPES experiments with the use of different photon energies in the 1st SBZ [28,29]. In Figs. 2(b) and 2(d) the calculated electronic spectra for Bi_2Te_2Se and Bi_2Se_2Te surfaces are shown in the same energy range used for the measured spectra given in Figs. 2(a) and 2(c), respectively. In the same panel the intensity maxima of one TSS branch above E_D obtained from momentum and energy distribution curves (EDCs) are also highlighted.

The calculated E_D are matched with those obtained by ARPES. The theoretical band dispersions above E_D for both Bi_2Te_2Se and Bi_2Se_2Te are in excellent agreement with those measured. In Bi_2Te_2Se the calculated TSS band crossing lies close to the valence band and thus dispersion of the lower TSS does not reproduce the experimental feature. On the other hand, in Bi_2Se_2Te the calculated dispersion below E_D well reproduces the measured linear dispersion of the TSS. The origin of the discrepancies between theoretical and experimental energy dispersions in the lower TSS for Bi_2Te_2Se might be ascribed to the presence of defects in the topmost Te layer that would move E_D away from the bulk valence band towards the gap center [39].

The group velocity at the Fermi energy (Fermi velocity) is estimated by the formula $1/\hbar(\partial E/\partial k)$ to be $(5.8 \pm 0.2) \times 10^5$ m/s in Bi_2Te_2Se and $(6.1 \pm 0.2) \times 10^5$ m/s in Bi_2Se_2Te. Also, Table I shows that the group velocity (v_g) near E_D is larger for Bi_2Te_2Se than for Bi_2Se_2Te. The value at E_D for Bi_2Te_2Se is close to $v_g = 4.6 \times 10^5$ m/s above 130 meV from E_D estimated by a magnetotransport measurement [30]. Here, the v_g near E_D is larger than that for Bi_2Se_3 ($v_g = 2.9 \times 10^5$ m/s), while the Fermi velocity is smaller ($v_g = 6.6 \times 10^5$ m/s) [10,15]. The TSSs in existing TI materials usually deviate from a linear dispersion when moving away from E_D. The ratios of v_g at E_F with respect to that at E_D for Bi_2Te_2Se and Bi_2Se_2Te are found to be 1.4 and 1.6, respectively. These values are smaller than those of the other 3D TIs (1.8 for $TlBiSe_2$ and 2.3 for Bi_2Se_3 though their E_D are deeper than in the present case), which means that the surface band dispersions for Bi_2Te_2Se and Bi_2Se_2Te possess a wider energy range where the linearly dispersive feature is maintained above E_D.

TABLE I. Binding energy at the Dirac point (E_D), group velocity at E_D and at the Fermi energy (E_F) of Bi_2Te_2Se and Bi_2Se_2Te.

E_D [meV]	$v_g(E_D) \times 10^5$ [m/s]	$v_g(E_F) \times 10^5$ [m/s]
415 ± 3	4.2 ± 0.4	5.8 ± 0.2
425 ± 3	3.7 ± 0.2	6.1 ± 0.2

To unravel the spin character and make a quantitative analysis of the spin polarization in these TSSs, we have performed SARPES measurement. Figures 3(a) and 3(b) show the spin-resolved EDCs of Bi_2Te_2Se and Bi_2Se_2Te. Here, the spin-up and -down spectra are plotted with triangles pointing up and down, respectively. Let us first take a look at the spin-resolved EDCs of Bi_2Te_2Se. A spin-up peak near E_F at $\theta = 49.5°$ shifts to higher E_B with increasing θ. A spin-down peak at 0.57 eV emerges at $\theta = 51.5°$ and moves to lower E_B with increasing θ. These spin-up and -down peaks are merged at $\theta = 56°$ corresponding to $\bar{\Gamma}_{2nd}$ ($E_B = 0.4$ eV). This result clearly shows that the TSS is spin-split and the spin orientations are antisymmetric with respect to the $\bar{\Gamma}$ point. For the peak originating in the bulk conduction band near E_F for $\theta = 53.5°$–$58.5°$, the spin-down intensity is larger than that in the spin-up channel. It might originate from the final state effect (matrix element effect) in the presence of spin-orbit coupling [40] (see Supplemental Material [41]). The observed features of the band dispersion and the spin polarizations in Bi_2Se_2Te are similar to those in Bi_2Te_2Se as shown in Fig. 3(b). Figures 3(c) and 3(d) depict the observed spin-up and -down peaks in Figs. 3(a) and 3(b) with triangles pointing up and down, respectively.

Importantly for the TSS, when there are clear peak structures in one spin channel, those in the opposite spin channel are weak or negligible in a similar energy range below $\theta = 55°$ ($\theta = 56.5°$) for Bi_2Te_2Se (Bi_2Se_2Te) [see Figs. 3(a) and 3(b)]. Here, it is noticed that the intensities of the lower part of the TSS in the spin-down channel at $\theta = 58.5°$ ($\theta = 59.5°$) of Bi_2Te_2Se (Bi_2Se_2Te) appear to be comparable to that in the spin-up channel due mainly to a superposition of the broad tail from the upper part of TSS with the same spin component. It turns out, however, that the spin-down intensity is intrinsically small compared to that in the spin up channel after an appropriate background subtraction procedure (see Supplemental Material [41]). The results clearly show the presence of surface Dirac fermions with a high degree of spin polarization in the bulk energy gap region. In fact, the TSS in Bi_2Te_2Se (Bi_2Se_2Te) maintains a high spin polarization of more than 40% (50%) over a wide energy region across E_D, though a nonpolarized inelastic background contributes to the total intensity. Here, the spin polarizations are corrected from the raw data by subtracting the constant and unpolarized background from the originally derived spin-up and spin-down spectra [21]. In particular, the spin polarization of TSS near E_F with a smaller background contribution Bi_2Te_2Se (Bi_2Se_2Te) reaches to more than 70% (50%). It was, however, quite difficult to estimate accurate values of spin polarizations near E_F in the measurement with a He lamp due to the overlap of the additional signal with considerable spin polarizations excited by the higher-energy satellite (β) line ($h\nu = 23.08$ eV). Therefore, we have tried to use SR to extract accurate

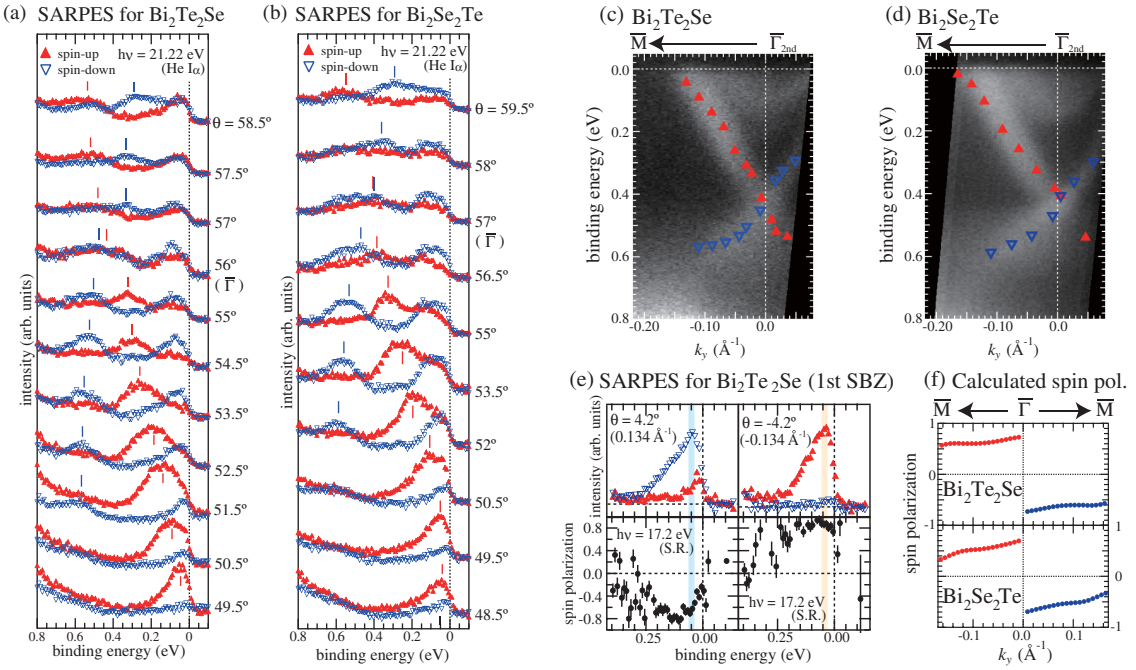

FIG. 3 (color). (a),(b) Spin-resolved energy distribution curves (EDCs) of Bi_2Te_2Se and Bi_2Se_2Te along the $\overline{\Gamma M}$ line obtained with unpolarized He-$I\alpha$ radiation. (c),(d) $E - k$ mapping by ARPES measurements with a He lamp. The spin characters derived from the spin-resolved spectra in Figs. 3(a) and 3(b) are superimposed. Here, k_y is measured from the $\bar{\Gamma}_{2nd}$ point. (e) Spin-resolved energy distribution curves and spin polarizations of Bi_2Te_2Se at $\theta = \pm 4.2°$ taken with p-polarized synchrotron radiation ($h\nu = 17.2$ eV). (f) Theoretical spin polarization values as a function of the wave vector obtained by the first principles calculation for the upper part of TSS in Bi_2Te_2Se and Bi_2Se_2Te. Spin-up and spin-down characters are denoted with triangles pointing up (red) and down (blue) in panels (a)–(e).

values. Figure 3(e) shows the SARPES results for Bi_2Te_2Se obtained by the monochromatic SR light ($h\nu = 17.2$ eV). As shown in the lower panel of Fig. 3(e), the magnitude of the spin polarization for the surface state reaches $87 \pm 9\%$ at $\theta = -4.2°$ and $-67 \pm 3\%$ at $\theta = 4.2°$. The difference of spin polarizations in positive and negative θ is probably derived from matrix elements for optical transitions. If the final-state spin polarizations are assumed to be equal in positive and negative θ near $\bar{\Gamma}$, an averaged spin polarization of $77 \pm 5\%$ is regarded as the absolute value of the initial-state spin polarization. Figure 3(f) shows the theoretical spin expectation values as a function of the wave vector (k_y) for the upper TSS in Bi_2Te_2Se and Bi_2Se_2Te obtained from the first principles calculation. Here, we find that the theoretical spin polarization for Bi_2Te_2Se (Bi_2Se_2Te) increases closer to the $\bar{\Gamma}$ point and reaches a maximum value of $\sim 75\%$ ($\sim 70\%$) at $\bar{\Gamma}$. Note that the spin polarization cannot reach 100% because the spin angular momentum is not a good quantum number any more due to the strong spin-orbit entanglement reported for Bi_2Te_3 and Bi_2Se_3 [34]. The experimentally evaluated spin polarization (77%) for TSS in Bi_2Te_2Se at $k_y = \pm 0.134$ Å^{-1} is larger than the theoretical value ($\sim 61\%$). It is worth noting that the latter is higher in Bi_2Te_2Se as compared with Bi_2Te_3, where the reversed spin direction was found at the outer Te atom [42,43]. In contrast to that in Bi_2Te_2Se, the layer projected spin analysis revealed identical spin helicity for all atomic layers. Moreover, the spin polarization near E_D is expected to have a higher value than those near E_F as the calculated spin polarization implies, although, as mentioned above, it is difficult to experimentally evaluate an accurate value of the spin polarization near the Dirac point.

In conclusion, the helical spin texture and the spin polarizations of the TSS in the ternary tetradymite chalcogenides Bi_2Te_2Se and Bi_2Se_2Te have been experimentally revealed by SARPES measurements. The markedly high spin polarization of the TSSs has been found to be $\sim 77\%$ and is persistent in a wide energy range across the Dirac point in those compounds. The availability of both upper and lower TSSs promises to extend the variety of spintronic applications, for instance, to the topological p-n junction and the dual gate TI device [32,34].

We thank Shuichi Murakami for valuable comments. This work was financially supported by KAKENHI (Grants Nos. 19340078, 20340092, 23340105, and 23244066), Grant-in-Aid for Scientific Research (A) and (B) of JSPS. K. A. K. and O. E. T. acknowledge financial support by the RSSF and RFBR (Grant No. 12-02-00226). The measurement was performed with the approval of the Proposal Assessing Committee of HSRC (Proposal No. 11-B-12).

*kmiyamoto@hiroshima-u.ac.jp

[1] L. Fu and C. L. Kane, Phys. Rev. B **76**, 045302 (2007).
[2] L. Fu, C. L. Kane, and E. J. Mele, Phys. Rev. Lett. **98**, 106803 (2007).
[3] X. L. Qi, T. L. Hughes, and S. C. Zhang, Phys. Rev. B **78**, 195424 (2008).
[4] M. Z. Hasan and C. L. Kane, Rev. Mod. Phys. **82**, 3045 (2010).
[5] X.-L. Qi, R. Li, J. Zang, and S.-C. Zhang, Science **323**, 1184 (2009).
[6] L. Fu and C. L. Kane, Phys. Rev. Lett. **100**, 096407 (2008).
[7] Y. L. Chen *et al.*, Science **325**, 178 (2009).
[8] H. Zhang, C.-X. Liu, X.-L. Qi, X. Dai, Z. Fang, and S.-C. Zhang, Nature Phys. **5**, 438 (2009).
[9] Y. Xia, D. Qian, D. Hsieh, L. Wray, A. Pal, H. Lin, A. Bansil, D. Grauer, Y. S. Hor, R. J. Cava, and M. Z. Hasan, Nature Phys. **5**, 398 (2009).
[10] K. Kuroda *et al.*, Phys. Rev. Lett. **105**, 076802 (2010).
[11] B. Yan, C.-X. Liu, H.-J. Zhang, C.-Y. Yam, X.-L. Qi, T. Frauenheim, and S.-C. Zhang, Europhys. Lett. **90**, 37002 (2010).
[12] H. Lin, R. S. Markiewicz, L. A. Wray, L. Fu, M. Z. Hasan, and A. Bansil, Phys. Rev. Lett. **105**, 036404 (2010).
[13] S. V. Eremeev, G. Bihlmayer, M. Vergniory, Y. M. Koroteev, T. V. Menshchikova, J. Henk, A. Ernst, and E. V. Chulkov, Phys. Rev. B **83**, 205129 (2011).
[14] T. Sato, K. Segawa, H. Guo, K. Sugawara, S. Souma, T. Takahashi, and Y. Ando, Phys. Rev. Lett. **105**, 136802 (2010).
[15] K. Kuroda *et al.*, Phys. Rev. Lett. **105**, 146801 (2010).
[16] Y. L. Chen *et al.*, Phys. Rev. Lett. **105**, 266401 (2010).
[17] D. Hsieh *et al.*, Nature (London) **460**, 1101 (2009).
[18] S. Souma, K. Kosaka, T. Sato, M. Komatsu, A. Takayama, T. Takahashi, M. Kriener, K. Segawa, and Y. Ando, Phys. Rev. Lett. **106**, 216803 (2011).
[19] S.-Y. Xu *et al.*, arXiv:1101.3985.
[20] Z.-H. Pan, E. Vescovo, A. V. Fedorov, D. Gardner, Y. S. Lee, S. Chu, G. D. Gu, and T. Valla, Phys. Rev. Lett. **106**, 257004 (2011).
[21] C. Jozwiak *et al.*, Phys. Rev. B **84**, 165113 (2011).
[22] P. Cheng *et al.*, Phys. Rev. Lett. **105**, 076801 (2010).
[23] T. Hanaguri, K. Igarashi, M. Kawamura, H. Takagi, and T. Sasagawa, Phys. Rev. B **82**, 081305 (2010).
[24] J. G. Checkelsky, Y. S. Hor, M.-H. Liu, D.-X. Qu, R. J. Cava, and N. P. Ong, Phys. Rev. Lett. **103**, 246601 (2009).
[25] N. P. Butch, K. Kirshenbaum, P. Syers, A. B. Sushkov, G. S. Jenkins, H. D. Drew, and J. Paglione, Phys. Rev. B **81**, 241301(R) (2010).
[26] K. Eto, Z. Ren, A. A. Taskin, K. Segawa, and Y. Ando, Phys. Rev. B **81**, 195309 (2010).
[27] D.-X. Qu, Y. S. Hor, J. Xiong, R. J. Cava, and N. P. Ong, Science **329**, 821 (2010).
[28] M. Neupane *et al.*, Phys. Rev. B **85**, 235406 (2012).
[29] T. Arakane, T. Sato, S. Souma, K. Kosaka, K. Nakayama, M. Komatsu, T. Takahashi, Z. Ren, K. Segawa, and Y. Ando, Nature Commun. **3**, 636 (2012).
[30] Z. Ren, A. A. Taskin, S. Sasaki, K. Segawa, and Y. Ando, Phys. Rev. B **82**, 241306(R) (2010).
[31] L. L. Wang and D. D. Johnson, Phys. Rev. B **83**, 241309 (R) (2011).
[32] J. Wang, X. Chen, B. F. Zhu, and S. C. Zhang, Phys. Rev. B **85**, 235131 (2012).
[33] K. Segawa, Z. Ren, S. Sasaki, T. Tsuda, S. Kuwabata, and Y. Ando, Phys. Rev. B **86**, 075306 (2012).
[34] O. V. Yazyev, J. E. Moore, and S. G. Louie, Phys. Rev. Lett. **105**, 266806 (2010).
[35] K. A. Kokh, B. G. Nenashev, A. E. Kokh, and G. Yu. Shvedenkov, J. Cryst. Growth **275**, e2129 (2005).
[36] T. Okuda, K. Miyamaoto, H. Miyahara, K. Kuroda, A. Kimura, H. Namatame, and M. Taniguchi, Rev. Sci. Instrum. **82**, 103302 (2011).
[37] G. Kresse and J. Furthmüller, Comput. Mater. Sci. **6**, 15 (1996).
[38] G. Kresse and D. Joubert, Phys. Rev. B **59**, 1758 (1999).
[39] S. V. Eremeev, Y. M. Koroteev, and E. V. Chulkov, JETP Lett. **91**, 387 (2010).
[40] R. Feder, *Polarized Electrons in Surface Physics* (World Scientific, Singapore, 1985).
[41] See Supplemental Material at http://link.aps.org/supplemental/10.1103/PhysRevLett.109.166802 for spin polarization of bulk and topological surface states.
[42] S. V. Eremeev *et al.*, Nature Commun. **3**, 635 (2012).
[43] J. Henk, A. Ernst, S. V. Eremeev, E. V. Chulkov, I. V. Maznichenko, and I. Mertig, Phys. Rev. Lett. **108**, 206801 (2012).